Characterization of Forests in Western Sayani Mountains, Siberia from SAR data

K. J. Ranson[1], G. Sun[2], V. I. Kharuk[3], and K. Kovacs[2]

[1]NASA's Goddard Space Flight Center, Code 923, Greenbelt, MD 20771 USA

Phone: (301) 286-4041, Fax: (301) 286-0239, E-mail: jon@taiga.gsfc.nasa.gov

[2]Department of Geography, University of Maryland, College Park, MD 20742 USA

[3]Sukachev Institute of Forest, Krasnoyarsk, Russia

Abstract-This paper investigated the possibility of using spaceborne radar data to map forest types and logging in the mountainous Western Sayani area in Siberia. L and C band HH, HV, and VV polarized images from the Shuttle Imaging Radar – C instrument were used in the study. Techniques to reduce topographic effects in the radar images were investigated. These included radiometric correction using illumination angle inferred from a digital elevation model, and reducing apparent effects of topography through band ratios. Forest classification was performed after terrain correction utilizing typical supervised techniques and principal component analyses. An ancillary data set of local elevations was also used to improve the forest classification. Map accuracy for each technique was estimated for training sites based on Russian forestry maps, satellite imagery and field measurements. The results indicate that it is necessary to correct for topography when attempting to classify forests in mountainous terrain. Radiometric correction based on a DEM improved classification results but required reducing the SAR resolution to match the DEM. Using ratios of SAR channels that include cross-polarization improved classification and

had the advantages of eliminating the need for a DEM and preserving the full resolution of the SAR data.

I. INTRODUCTION

The usefulness of SAR for mapping forests has been demonstrated by several authors using different systems over various forest types (e.g., Ranson and Sun, 1997a-b; Ranson et al., 1995; Rignot et al., 1994; Dobson et al., 1996; Saatchi and Rignot, 1997; Pierce et al., 1998). These studies, however, were all conducted in areas with low topographic relief. Since a significant amount of the world's forests grow in mountainous areas, techniques to effectively utilize SAR are needed. High-resolution optical remote sensing data such as SPOT and Landsat have been used to map mountainous terrain, where the techniques utilize normalization with a DEM (Franklin 1991), band ratios (Colby 1991), and radiation scattering models (Franklin 1991; Colby and Keating 1998) were used.

Topography greatly influences the radar backscatter through local incidence angle, shadowing, and layover effects (Leberl 1990). The terrain effects on radar backscattering are complex. Because of the slope, the radar incidence angle changes. The change of radar incidence angle has several effects on radar imaging data: a) for a certain target, radar backscattering is a function of incidence angle; and b) the target area (so the number of scatterers) imaged by a radar slant pixel depends on incidence angle, i.e. smaller incidence angle means more ground surface areas are being imaged by the radar image pixel (foreshortening); c) if the slope is larger than the nominal radar incidence angle, layover happens, and the backscattering from the slope will mix with signature from other targets. When the back slope is larger than the incidence angle, shadow occurs. There is no way to recover the signature lost due to layover and shadowing. The terrain-

effect correction techniques are designed to reduce effects a) and b) listed above. For correction of effect b), i.e. the pixel area correction, a simple algorithm could be used if a DEM exists (Shi and Dozier, 1997; Kellndorfer et al. 1998). For correction of effect a), the dependence of backscattering on incidence angle needs to be known for the pixel to be corrected, which requires knowing the land cover type of this pixel. This is a dilemma because knowing the cover type of the pixel is required for choosing appropriate radar backscatter model for incidence angle effect correction, but the purpose of terrain-correction is for image classification, i.e. deriving land cover types from radar images. Few attempts have been made by using simple radar backscattering models and DEM. For example, Goering et al. (1995) used a DEM and empirical radar backscatter models to reduce terrain effects from ERS-1 SAR images. Researchers (Goyal et al., 1998) have found that the small-scale topographic features resolved by SAR couldn't be resolved by a DEM in rugged terrain. Periodic artifacts due to the terrain model generation methodology were observed in the derived variables (e.g slopes). Other methods, such as image ratios were used to reduce the effects of radar incidence angle caused by topography (Ranson et al., 1995; Shi and Dozier, 1997; Wever and Bodechtel 1998). Wever and Bodechtel (1998) also proposed to use LHV and XVV ratio or difference images for radiometric rectification.

Within the Siberian region where our study located mountainous areas comprise about 50% of the forested terrain. Generally, high resolution optical data have not been used to map and monitor this area, because of the frequent cloud cover, low Sun angle, and lack of local ground receiving stations. (This is now changing with the April 15, 1999 launch of Landsat 7). Radar data with its ability to penetrate clouds promises to useful for monitoring forests and other landscapes in this area if terrain effects can be reduced. In this study, the terrain-correction by use of DEM and image ratios on forest classification are presented and discussed.

II. STUDY AREA

The Western Sayani test area covers a 50 x 25 km area with center coordinates of 53° 4.2' N latitude and 93° 14.3' E longitude (Fig. 1). The area is part of the dark-coniferous taiga forests that grow in mountainous regions (300-1700 m above mean seal level). The forests of this area include cedar (*Pinus siberica*), fir (*Abies sibirica*), aspen (*Populus tremula*) and birch (*Betula verrocosa*, B.*pubescens*, *Betula spp.*). The climate is continental with wet summers and cold dry winters. Temperature and precipitation are strongly controlled by elevation. Annual precipitation varies from 560 mm in the lower regions to 1300 mm at higher elevations. Tree-line occurs at about 1400 m elevation. The area is the site of the Ermakovsky Permanent Study Area established in 1959 and used for research by the Sukachev Institute of the Siberian Branch of the Russian Academy of Sciences.

A Russian forest inventory map (1:50,000) compiled from aerial photographs and field checks between 1993 and 1995 was used as ground truth information. The map is typical of forest inventory maps with forest units related to economic value of the stands. Table 1 lists the land cover classes used in this analysis. The forest map contained an intermediate age class for some of the forest categories. Because of the paucity of these sites and the related difficulties encountered in finding adequate training areas this age class was not included. A reduced set of classes was developed by combining deciduous and conifer species types, however, old and young designations were retained. This resulted in 12 cover classes, evenly split between forested and non-forested classes as listed in Table 1.

III. SIR-C/XSAR

The satellite data used in this study was synthetic aperture radar (SAR) data from the Shuttle Imaging Radar/ X-band SAR (SIR-C/XSAR) mission. SIR-C/X-SAR was part of a series of spaceborne imaging radar missions that began with the June 1978 launch of Seasat SAR and continued with the November 1981 SIR-A and October 1984 SIR-B missions. The SIR-C/X-SAR missions were successfully conducted during April 9-19, 1994 and September 30-October 10, 1994 and demonstrated the design and capabilities of a spaceborne multifrequency polarimetric SAR (Stofan et al., 1995). The instrument had quad-polarized (HH,HV,VV,HV) L-band (wavelength =23 cm) and C-band (5.6 cm) radar and VV polarized X-band (3 cm) radar channels. The SIR-C/X-SAR design included bandwidths of 10, 20, and 40 MHz. The instrument augmented the present and still current configurations of orbiting radar systems such as the C-band VV-polarized ERS-1, and C-band HH-polarized RADARSAT and the (now defunct) L-band HH polarized JERS-1 systems. The mission was a cooperative experiment between NASA's Jet Propulsion Laboratory (JPL), the German Space Agency, and the Italian Space Agency. SIR-C/X-SAR was launched on space shuttle Endeavour and acquired multiple data takes covering over 6% of the Earth's surface including a variety of land, ocean and ice targets.

IV. METHODS

The methods employed in this work involved comparing approaches for reducing topographic effects on forest classification and utilizing ancillary information including topography to produce the best classification possible for forested mountainous terrain. This section discusses radiometric correction after computing local incidence angle from a DEM and topographic effect reduction using SAR channel ratios. The best method was selected and used with the ancillary data to further improve the classification.

Radiometric Correction With A Digital Elevation Model

For this study area, the DEM available for use was Digital Terrain Elevation Data (DTED) Level 1 (3 arc second pixel spacing) from the US Department of Defense. The DEM offers a pixel spacing of roughly 100 by 100 m and a nominal accuracy of ± 30 m. The use of low-resolution DEM for geocoding and radiometric correction of the higher resolution radar images (~30m) was unsatisfactory because of the difficulty in matching control points. Therefore, the resolution of the radar images was reduced to the resolution of DEM. To facilitate identification of control points on both SAR and DEM images a radar image was simulated based on the DEM and the mission, sensor, and image parameters provided by JPL (Table 2). Ground control points were selected from both SIR-C and simulated SAR images and used to orthorectify and geocode the radar images to the DEM. Slope and aspect were generated from DEM and used to calculate the local incidence angle for every pixel of the image.

The SIR-C image data used in this study were acquired on April 16, 1994 with an imagge center incidence angle of 46.4° and bandwidth of 10 MHz. The SAR channels used were L-band and C-band with HH,HV and VV polarizations. (VH was not included because it was redundant with HV). The L- and C-band images (LHH, LHV, HVV, CHH, CHV, CVV) were processed with 6 looks in azimuth and converted from slant to ground range resulting in a pixel size of ~30m. To reduce image speckle, the images were filtered using a Lee filter with a 5X5 pixel window as described in PCI (1997). Figure 2 is the LHV image of the test site showing obvious topography effects. The resolution of the SIR-C image data was reduced to about 50m by spatial averaging and registered to the DEM simulated image. Registration was accomplished with 21 control points and a first order nearest neighbor resampling routine of PCI (1997).

Slope and aspect were generated from the DEM and used to calculate the local incidence angle for every pixel of the image as:

$$\cos(i) = \cos(a_s)*\cos(a) + \sin(a_s)*\sin(a)*\cos(\alpha-\alpha_s) \quad (1)$$

where i = local incidence angle

a_s = local slope angle

a = incidence angle of SAR beam at the center of image

α_s = aspect of slope (if North = 0 deg)

α = azimuth angle of SAR beam

Radiometric distortion due to the illumination area was corrected using this angle by the equation used by Kellndorfer et al. (1998):

$$I_{corr} = DN*(\sin(i)/(\sin(i_{ref})) \quad (2)$$

where: I_{corr} = radar signal intensity corrected for local incidence angle

DN = digital number of pixel in intensity format

i = local incidence angle at each pixel

i_{ref} = the radar incidence angle at the center of the image

Kellndorfer et al. (1998) have found that this correction was adequate for land cover classification purposes. Fig. 3 is the LHV image corrected in this manner. Because of the low resolution of the available DEM data, the results obtained do not appear to be very satisfactory since there are residual topographic effects in the image. Because the best available DEM data was used and there was reduction in the overall topographic features this approach was applied to all six SAR channels to produce radiometrically "corrected" images. In the future, new data sets such as that from the Shuttle Radar Topography Mission (SRTM) should improve the DEM quality.

Forest Classification

Training areas for each of the original map classes were identified on the forestry maps and located on the SAR images. A SPOT HRV image acquired in August 11, 1991 and a 1983 Russian Resours F image were also used to assist in identifying training sets. The initial classification approach used the six uncorrected SIR-C channels in a supervised maximum likelihood classifier available with the PCI analysis system. The second classification used a similar method with the 6 channels of SAR data radiometrically corrected using Equations 1 and 2.

A third method of classification using selected band ratios was also used to attempt to reduce topographic effects. Of the thirty ratio combinations possible, there are six non-redundant single band combinations (e.g., LHH/LVV) and 9 non-redundant two-band combinations (e.g., LHH/CHV). It is obvious that the ratio reduces apparent topography while retaining some forest cover information as seen in the image presented in Figure 4. Three band ratios are used for the display: LHV/LVV (red), LHV/CVV (green) and LHH/LHV(blue).

Principal component analysis (PCA) was performed using the ratio data. Fig. 5 shows a color composite image of the first three principal components. First, the first four principal components of the ratio images (accounting for over 97% of the variation in the transformed data set, Table 3) were used in a supervised classification. Then the first six principal components were used. The addition of the last two components was selected to attempt to improve some forest type discrimination as discussed below. Classification maps were generated for the unocorrected data, radiometrically corrected and geocoded data and the principal components of ratio data. Comparisons of the results were made by examining the classification of the training data sets as discussed below.

V. RESULTS AND DISCUSSION

Uncorrected Data

The consequence of failing to consider the effects of topography when classifying mountainous landscapes is illustrated by the poor results obtained Table 4. Average classification accuracy was only 24% with some classes completely misclassified. Of course results with uncorrected data may be improved by selecting classes based on topography (e.g., front or rear facing slopes) but this was not done in order to maintain consistency across the classifications of SAR data. The error matrices of training sites showed that the confusion of forest type with clearcut and snow were severe making these results useless for forestry or ecology studies. Only the water training areas were classified with good results.

Table 5 lists the classification results obtained using the radiometric correction procedure described in the Methods section. Even though the correction algorithm was simple and dependent on the quality of the DEM and accuracy of image registration the results improved dramatically from the uncorrected results reported above. Average accuracy improved to over 72% with non-forest classes classification accuracy better than 80%. Forest type classification also improved, but there are still errors in discriminating between forest type and age classes. For example, over 25% of the young deciduous class was mislabeled as conifer and over 17% of old conifer (OC) was mislabeled as young conifer (YC). The water class accuracy decreased from the original classification with over 18% classified as wetland (WET). This was mostly due to a decrease in false alarm errors for wetland and rock classes. Since wetlands occur adjacent to water bodies there are also some mixed pixel or misregistration effects.

Because of the problems inherent in trying to register SAR data to digital elevation model data we decided to use SAR channel ratios to avoid the geometric and radiometric correction steps in the classification. SAR channel ratios have been shown in the past to reduce topographic effects (Ranson and Sun 1997b; Shi and Dozier 1997; Wever and Bodechtel 1998). Therefore we used the

available ratios developed from the six channels of SIR-C data as discussed above. The first four principal components were selected for the classification. The results are shown in Table 6 with average accuracy slightly better than radiometrically corrected data at 77%. However, forest type classification was seriously degraded compared to the previous example, especially for the old and young conifer classes. Young conifer classification accuracy was only about 39% (vs 59% for previous example, Table 5) with most confusion with young deciduous and old conifer. Old conifer was mostly confused with young conifer and young deciduous. Clearcut accuracy also fell from 85% to 65% with most confusion with old and young conifer.

An additional classification was attempted with the inclusion the fifth and sixth principal components. The rationale for adding these components was to increase sensitivity to forest structure by using PCs with co-polarized channels. Studies (Wu and Sader 1987; Paris and Woodruff 1991) have demonstrated that co-polarized ratios such as LHH/LVV are useful for identifying canopy structure differences (e.g., bole and branch arrangements). This ratio is also sensitive to the presence of trunk-ground interactions, because this interaction produces a larger HH/VV ratio (Durden et al., 1991; Sun et al., 1991). Fig. 6 is the classification map from sx principal components. The classification results are listed in Table 7. Average accuracy improved slightly to about 81% with excellent results for non-forest classes. Forest discrimination improved with old deciduous accuracy increasing to nearly 87%. Young deciduous classification performance improved 10%, but still was confused with other forest classes 25% of the time. Young and old conifer improved over the 4 PC analysis, but were still too low (~50 to 60%) to be useful for mapping studies. Again these classes were mostly misclassified with each other or young deciduous.

The poor classification of the conifer classes is a serious problem if the mapped results are to be of use to forest scientists or managers. Since the purpose of this study was to compare classification techniques, the resolution used was kept consistent at about 50m. This resolution was dictated by the resolution of the DEM used earlier for radiometric correction. However, it is not necessary to use this degraded resolution for the channel ratio classification approach. Potentially, better resolution could yield better results. Therefore we reclassified the forest area using the 6 PC data and full resolution data. Improving the resolution also improved the classification results for the conifer classes (Table 8). Deciduous results were mixed with young deciduous results improving, but old deciduous getting worse. Also of note is the dramatic increase in the alpine shrub classification (77% to 98%).

So far the results indicate that a DEM is useful for radiometric correction, but that ratios can be used to better improve classification accuracy. However, knowledge of topography can also be used to modify a classification based on knowledge of forest ecology. A straight forward way to do this is to use the known elevational limits of growth for forest species. For example, based on field surveys in the Sayani Mountains aspen and birch do not grow above 650m elevation and the highest elevation supporting tree growth (i.e., tree line) has been identified as 1400m. By applying some simple rules the classification can be modified to reflect these limits. We did this by employing decision rules:

If old image class = YD and elevation is :> 650m then new image class = YC

If old image class = OD and elevation is :> 650m then new image class = OC

For cases of forest misclassified above tree line if forest is identified as young deciduous or young conifer then it is changed to alpine shrub, if misclassified as old forest then its is labeled as unkown since there is no logical class to replace it with.

If old image class = YD and elevation is > 1400m then new image class = SHR

If old image class = YC and elevation is > 1400m then new image class = SHR

If old image class = OD and elevation is > 1400m then new image class = Unknown

If old image class = OC and elevation is > 1400m then new image class = Unknown

If old image class = Mix and elevation is > 1400m then new image class = Unknown

Table 9 shows that young deciduous changed the most with 2.4% of the original pixels classified as YD converted to YC and about 2% of the OC being converted to OC. However, the overall effect of imposing these rules on the classification was less than 5%.

VI. SUMMARY and CONCLUSIONS

This work has demonstrated that effects of topography on forest classification in mountains terrain are important and must be considered. We approached the problem two ways. 1) radiomteric correction using a DEM and 2) using band ratios to reduce the topography effect in the SAR data. Radiometric correction using a simple algorithm substantially improved classification despite dependence on a poor quality DEM. PCA with 15 band ratios provided the best classification when selecting the first six PCs. Using the higher resolution data for band ratios and PCA produced the best classification. This demonstrated that high resolution radar (e.g ~30 m) may be necessary to discriminate some forest classes such as old conifer. Old conifers in the study area are mapped as economically important and stands can be labeled even though only a few large trees exist in the stand.

Topographic information can be used to reduce misclassifications when species elevation limits are known. A high quality DEM such as that to be acquired by the Shuttle Topographic

Mapping Mission in February 2000 is required to be able to use this information most effectively. Radiometric correction would also yield better results given a better DEM.

The techniques and approaches discussed here that utilize SIR-C data cannot, at this time be used since no operational satellite exists with multiple C- and L-Band channels. There are plans to launch C-band multichannel SAR by Canada (Radarsat) and Europe (Envisat ASAR) and multi-channel L-band SAR (ALOS PALSAR) by Japan. While these data will be useful there will still be difficulties due to the fact the data must be registered to use between satellite platforms.

ACKNOWLEDGMENTS

The study was supported partially by NASA HQ Office of Earth Science NASA grant NAG-5-3548.

REFERENCES

Colby, J.D., (1991), Topographic normalization in rugged terrain. *Photogrammetric Engineering and Remote Sensing*, 57:531-537.

Colby, J.D. and P.L. Keating, (1998), Land cover classification using Landsat TM imagery in the tropical highlands: the influence of anisotropic reflectance. *International J., Remote Sensing*. 19:1479-1500.

Dobson, M. C., L.E. Pierce, and F.T. Ulaby, (1996), Knowledge-based land cover classification using ERS-1/JERS-1 SAR composites, *IEEE Transactions on Geoscience and Remote Sensing*, 34(1):83-99.

Durden, S. L., J. D. Klein, and H. Zebker, (1991), Polarimetric radar measurements of a forested area near Mt. Shasta, *IEEE Transactions on Geoscience and Remote Sensing*, Vol. 29, No. 3, pp. 444-450, 1991.

Franklin, S.E., (1991), Image transformations in mountainous terrain and the relationship to surface patterns. *Computers and Geoscienc*17:1137-1149.

Goering, D. J., H. Chen, L. D. Hinzman, and D. L. Kane, (1995), Removal of terrain effects from SAR satellite imagery of Arctic tundra, *IEEE Transactions on Geoscience and Remote Sensing*, Vol. 33, No. 1, pp. 185-194.

Goyal, S. K., M. S. Seyfried and P. E. O'Neill, (1998), Effect of digital elevation model resolution on topographic correction of airborne SAR, *Int. J. Remote Sensing*, Vol. 19, No. 16, pp. 3075-3096.

Leberl, F. W., (1990), *Radagrammetric Image Processing*. Artech House, Norwood, MA.

Kellndorfer, J, L.E. Pierce, M.C. Dobson, and F.T. Ulaby, (1998), Toward consistent regional-to-global-scale vegetation characterization using orbital SAR systems. *IEEE Transactions on Geoscience and Remote Sensing*, 36(5):1396-1411.

Paris, J. and R. Woodruff, (1991), Results from four years of field research with a C-band)6-cm) field microwave scatterometer in cultural- and natural-vegetation sites, *IGARSS'91*, pp. 2255-2256.

PCI, Inc., (1997), *Using PCI Software*, Version 6.1. Ontario, Canada.

Pierce, L. E., K. M. Bergen, M. C. Dobson, and F. T. Ulaby, (1998), Multitemporal land-cover classification using SIR-C/X-SAR imagery, *Remote Sensing of Environment*, 64(1): 20-33.

Ranson, K. J. and G. Sun, (1997a), Mapping of boreal forest biomass from spaceborn synthetic aperture radar, *Journal of Geophysical Research*, 102(D24):29,599-29,610.

Ranson, K. J. and G. Sun, (1997b), An evaluation of AIRSAR and SIR-C/X-SAR images for mapping Northern forest attributes in Main, USA, *Remote Sensing of Environment*, 59:203-222.

Ranson, K. J., S. Saatchi, and G. Sun, (1995), Boreal Forest Ecosystem Characterization with SIR-C/X-SAR, *IEEE Transactions on Geoscience and Remote Sensing*, 33(4):867-876.

Rignot, E.J.M., C.L. Williams, J.Way, and L.A. Viereck, (1994), Mapping forest types in Alaskan boreal forests using SAR imagery, *IEEE Transactions on Geoscience and Remote Sensing*, 32(5):1051-1059.

Saatchi, S. and E. Rignot, (1997), Classification of boreal cover types using SAR images, *Remote Sensing of Environment*, 60:270-281.

Shi, J. C and J. Dozier, (1997), Mapping seasonal snow with SIR-C/X-SAR in mountainous areas, *Remote Sensing of Environment*, Vol. 59, No. 2, pp. 294-307.

Stofan, E. R., D. L. Evans, C. Schmullius, B. Holt, J. J. Plaut, J. van Zyl, S. D. Wall and J. Way, (1995), "Overview of results of Spaceborne Imaging Radar-C, X-band Synthetic Aperture Radar (SIR-C/X-SAR)", *IEEE Transaction on Geoscience and Remote Sensing*, Vol. 33, No. 4, pp. 817-828.

Sun, G., D. S. Simonett, and A. H. Strahler, (1991), A radar backscatter model for discontinuous coniferous forests, *IEEE Transaction on Geoscience and Remote Sensing*, Vol. GE-29, No. 4, pp. 639-650.

Wever, T. and J. Bodechtel, (1998), Different processing levels of SIR-C/X-SAR radar data for the correction of relief induced distortions in mountainous areas, *International Journal of Remote Sensing*, 19(2):349-357.

Wu, S. T. and S. A. Sader, (1987), Multipolarization SAR data for surface feature delineation and forest vegetation characterization, *IEEE Transactions on Geoscience and Remote Sensing*, 25: 67-76.

Table 1. Forestry map classes and reduced for SAR analysis.

Map Class	Description	SAR Class(Code)
Clearcut	Recently cleared areas	Clearcut (CC)
Shrub	Low vegetation	Shrub (SHR)
Wetlands	vegetation in perpetually wet areas	Wetlands (WET)
Rock	Bare rock outcroppings	Rock (RCK)
Water	Open water in lakes and rivers	Water (WAT)
Snow	Snow covered areas	Snow (SNW)
Old Aspen	Mature stands of aspen	Old deciduous (OD)
Old Birch	Mature Stands of birch	
Young aspen	Immature stands of aspen	Young Deciduous(YD)
Young birch	Immature stands of birch	
Old cedar	Mature stands of Siberian pine (cedar)	Old Conifer (OC)
Old fir	Mature stands of Siberian fir	
Young cedar	Immature stands of Siberian cedar	Young Conifer (YC)
Young fir	Immature stands of Siberian fir	
Mixed forest	Forest stands with no dominant species present	Mixed forest (MIX)

Table 2. Radar parameters used for image simulation from DEM.

Output Pixel Size	26.649 m X 34.555 m
Platform Altitude	223.4574 km
Platform Heading Angle	71.1443329
Minimum Look Angle	46.08•
Location of First Pixel	53.1489372• N 92.7996979• E

Table 3. Eigenvalues and variation for the first 6 principal components.

PC	Eigenvalue	Variation, %
1	5.441	64.1
2	1.9412	22.9
3	0.4500	5.30
4	0.4011	4.73
5	0.1142	1.35
6	0.0766	0.90

Table 4. Classification results for six uncorrected SAR channels. Overall Accuracy = 15.2%, average accuracy = 24.6%.

	Total Pixels	YD	OD	YC	OC	MIX	SHR	WET	CC	RCK	SNW	WAT
YD	733	**0.0**	0.0	31.4	0.8	19.1	0.0	0.0	7.6	0.4	39.3	0.0
OD	1353	0.2	**3.1**	9.53	0.5	39.7	0.2	0.0	17.3	3.0	26.7	0.0
YC	421	0.5	0.7	**23.3**	0.9	21.6	1.16	0.0	16.6	1.9	34.4	0.0
OC	759	0.7	2.4	20.4	**1.7**	22.5	0.0	0.0	22.7	1.6	28.0	0.0
MIX	537	0.0	0.9	0.6	0.4	**49.9**	0.0	0.0	28.3	5.8	14.2	0.0
SHR	279	2.2	0.4	39.4	4.3	12.2	**0.0**	0.0	5.4	0.4	35.8	0.0
WET	1070	0.0	79.8	0.2	0.1	7.8	0.0	**0.0**	1.4	0.40	4.1	5.3
CC	556	0.0	15.6	11.9	0.9	13.9	0.2	0.0	**26.2**	5.4	25.9	0.0
RCK	200	0.0	40.0	0.0	0.0	3.5	0.0	0.0	3.0	**37.5**	14.0	2.0
SNW	381	0.0	0.00	3.9	2.3	25.2	0.0	0.0	6.6	0.00	**39.9**	0.0
WAT	208	0.0	12.5	0.0	0.0	0.00	0.0	0.0	0.0	0.0	0.0	**87.5**

Table 5. Classification results for six radiometrically corrected SAR channels. Overall Accuracy = 70.4%, average accuracy = 72.4%.

	Total Pixels	YD	OD	YC	OC	MIX	SHR	WET	CC	RCK	SNW	WAT
YD	733	**60.7**	5.2	12.1	13.4	0.0	8.50	0.0	0.1	0.0	0.0	0.0
OD	1353	6.3	**66.3**	5.3	2.4	15.0	0.2	0.0	4.1	0.0	0.5	0.0
YC	421	6.4	6.7	**57.0**	12.8	1.7	4.5	0.0	9.3	0.0	1.6	0.0
OC	759	7.1	5.9	17.4	**48.2**	2.7	4.9	0.0	13.2	0.0	0.8	0.0
MIX	537	0.2	8.9	3.2	0.4	**72.1**	0.0	0.0	12.6	0.0	2.6	0.0
SHR	279	18.7	0.0	11.1	12.5	0.0	**57.0**	0.0	0.70	0.0	0.0	0.0
WET	1070	0.0	1.7	1.5	0.2	0.0	0.0	**85.40**	11.1	0.10	0.0	0.0
CC	556	0.8	2.4	5.2	2.9	1.8	0.0	0.2	**85.0**	0.0	1.8	0.0
RCK	200	0.0	0.0	0.0	0.0	0.0	0.0	0.0	3.0	**95.0**	2.0	0.0
SNW	381	0.0	1.9	1.6	0.30	2.4	0.0	0.0	6.0	0.0	**87.9**	0.0
WAT	208	0.0	0.0	0.0	0.0	0.0	0.0	18.30	0.0	0.0	0.0	**81.7**

Table 6. Classification results for four principal components from band ratios. Overall accuracy - 74.7%, Average accuracy = 77.7%

	Total Pixels	YD	OD	YC	OC	MIX	SHR	WET	CC	RCK	SNW	WAT
YD	733	**59.90**	12.3	14.8	11.9	0.4	0.2	0.0	0.6	0.0	0.0	0.0
OD	1092	1.5	**75.8**	2.7	2.4	13.6	0.0	2.6	1.40	0.0	0.0	0.0
YC	421	18.0	5.0	**39.4**	30.6	0.3	0.5	0.0	5.2	0.0	0.2	0.0
OC	438	14.2	4.6	19.6	**54.8**	2.97	0.5	0.0	3.5	0.0	0.0	0.0
MIX	537	2.8	6.6	1.7	9.9	**76.0**	0.0	0.0	3.2	0.0	0.0	0.0
SHR	279	2.2	0.0	1.4	0.0	0.0	**96.1**	0.0	0.4	0.0	0.0	0.0
WET	1070	0.0	7.2	0.0	0.0	0.1	0.0	**92.6**	0.1	0.0	0.0	0.0
CC	556	1.1	3.4	13.0	10.3	6.9	0.2	0.0	**65.3**	0.0	0.0	0.0
RCK	146	0.0	0.0	0.0	0.0	0.0	0.0	1.4	0.	**98.6**	0.0	0.0
SNW	191	0.0	0.0	0.0	0.0	0.0	0.0	0.0	1.	0.0	**99.0**	0.0
WAT	208	0.0	0.0	0.0	0.0	0.0	0.0	2.9	0.	0.0	0.0	**97.1**

Table 7. Classification results for six principal components. Overall accuracy = 80.7%, average accuracy = 81.3%

	Total Pixels	YD	OD	YC	OC	MIX	SHR	WET	CC	RCK	SNW	WAT
YD	733	**69.2**	10.1	10.5	5.4	0.0	2.9	0.0	1.9	0.0	0.0	0.0
OD	1353	3.4	**86.7**	1.3	0.2	6.2	0.0	1.2	1.2	0.0	0.0	0.0
YC	421	12.8	6.7	**58.7**	18.5	0.0	1.7	0.0	1.7	0.0	0.0	0.0
OC	759	16.3	6.3	18.6	**50.8**	0.4	0.8	0.0	6.5	0.0	0.2	0.0
MIX	537	1.3	9.9	0.9	1.0	**83.1**	0.0	1.7	2.3	0.0	0.0	0.0
SHR	556	6.1	0.0	10.8	6.1	0.0	**77.1**	0.0	0.0	0.0	0.0	0.0
WET	279	0.0	3.0	0.0	0.0	0.0	0.0	**95.2**	0.0	0.0	0.0	1.8
CC	1070	0.0	0.6	4.8	2.4	0.7	0.0	0.0	**91.6**	0.0	0.0	0.0
RCK	200	0.0	0.0	0.0	0.0	0.0	0.0	6.5	0.0	**93.50**	0.0	0.0
SNW	381	0.0	1.8	1.1	0.0	0.0	0.0	0.0	0.5	0.0	**96.6**	0.0
WAT	208	0.0	0.0	0.0	0.0	0.0	0.0	9.1	0.0	0.0	0.0	**90.9**

Table 8. Classification results for six principal components at full spatial resolution (29m). Overall accuracy = 85.0%, average accuracy = 87.1%.

	Total Pixels	YD	OD	YC	OC	MIX	SHR	WET	CC	RCK	SNW	WAT
YD	1743	**75.3**	15.2	8.6	0.5	0.5	0.0	0.0	0.0	0.0	0.0	0.0
OD	2878	9.1	**82.5**	0.8	0.4	4.4	0.0	2.2	0.5	0.0	0.0	0.0
YC	853	13.2	2.3	**67.3**	14.3	0.0	1.2	0.0	1.7	0.0	0.0	0.0
OC	1526	0.8	0.3	18.1	**75.4**	0.5	0.0	0.0	4.8	0.0	0.1	0.0
MIX	1138	3.5	10.8	1.0	0.2	**81.5**	0.0	2.5	0.70	0.0	0.0	0.0
SHR	581	0.0	0.0	1.0	0.3	0.0	**98.6**	0.0	0.0	0.0	0.0	0.0
WET	2261	0.0	4.4	0.0	0.0	0.0	0.0	**95.2**	0.0	0.4	0.0	0.0
CC	1145	0.0	2.0	0.8	5.6	0.7	0.0	0.0	**90.8**	0.0	0.0	0.0
RCK	419	0.0	0.0	0.0	0.0	0.0	0.0	2.4	0.0	**97.6**	0.0	0.0
SNW	839	0.0	0.0	1.7	0.0	0.0	0.0	0.5	0.0	0.0	**97.9**	0.0
WAT	435	0.0	0.0	0.0	0.0	0.0	0.0	3.4	0.0	0.9	0.0	**95.6**

Table 9. Effect of applying elevation rules on image classification.

Forest Type	% of Old Image Occupied	% of Image Modified	New Class
YD	12.05	2.38	YC
OD	19.84	1.73	OC
YD	12.05	0.0	SHR
YC	14.6	2.39	SHR
OD	19.84	0.22	Unknown
OC	11.03	1.82	Unknown
MIX	4.14	0.05	Unknown

Figure Captions

Figure 1. Map of test area location
Figure 2 LHV image of the Sayani test site showing mountains on right side.
Figure 3. Terrain-effect corrected LHV image using the DEM.
Figure 4. Composite image of Sayani test site using ratio of SIR-C Channels: LHH/LVV = red, LHV/CVV = green, and LHH/LHV = blue.
Figure 5. Composite image produced from first three principal components of SIR-C ratio images.
Figure 6. Classification image with 6 principal components.

Figure 2. LHV SAR image of the Sayani test site showing mountains on right side.

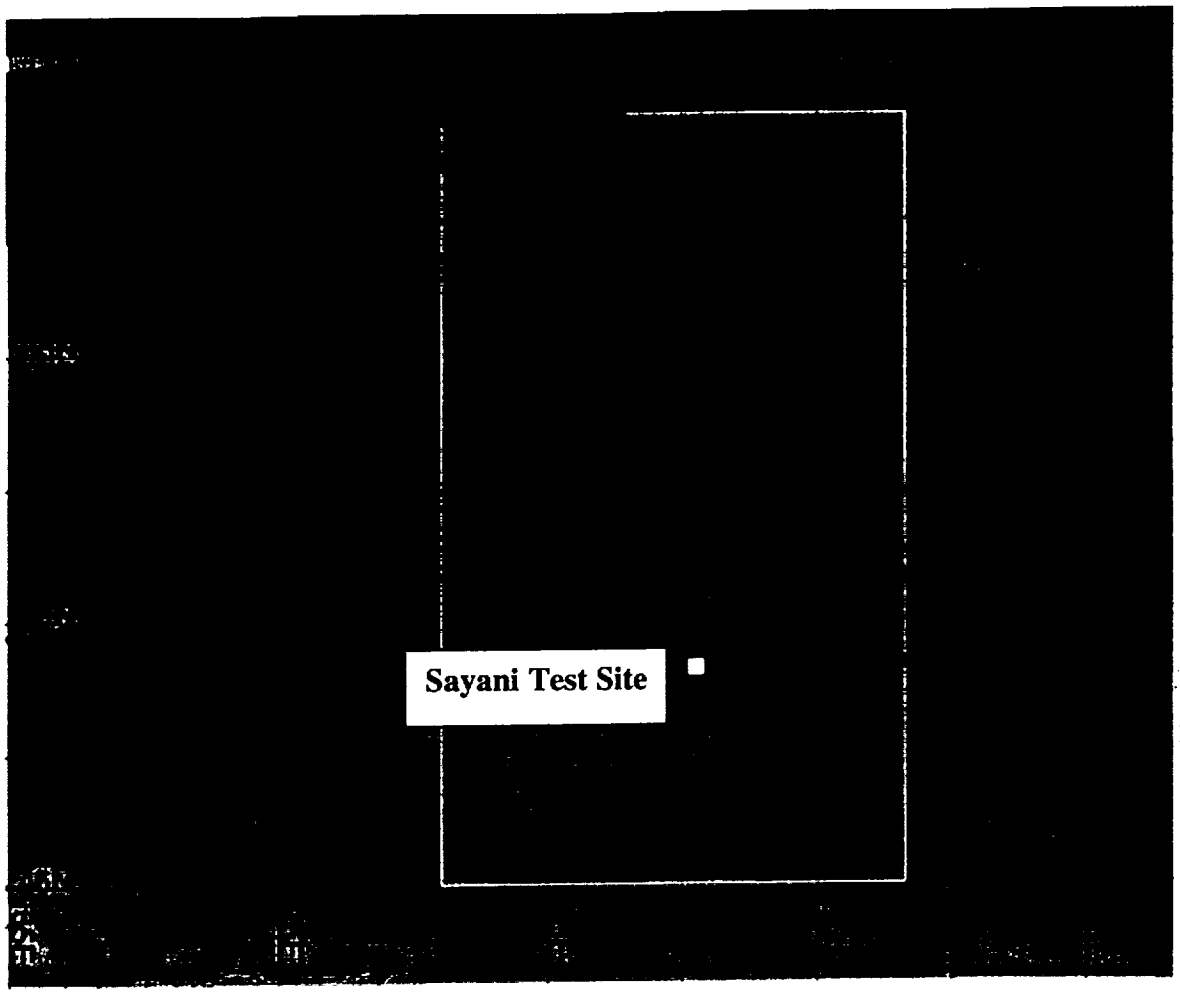

Figure 1. Map of test area location.

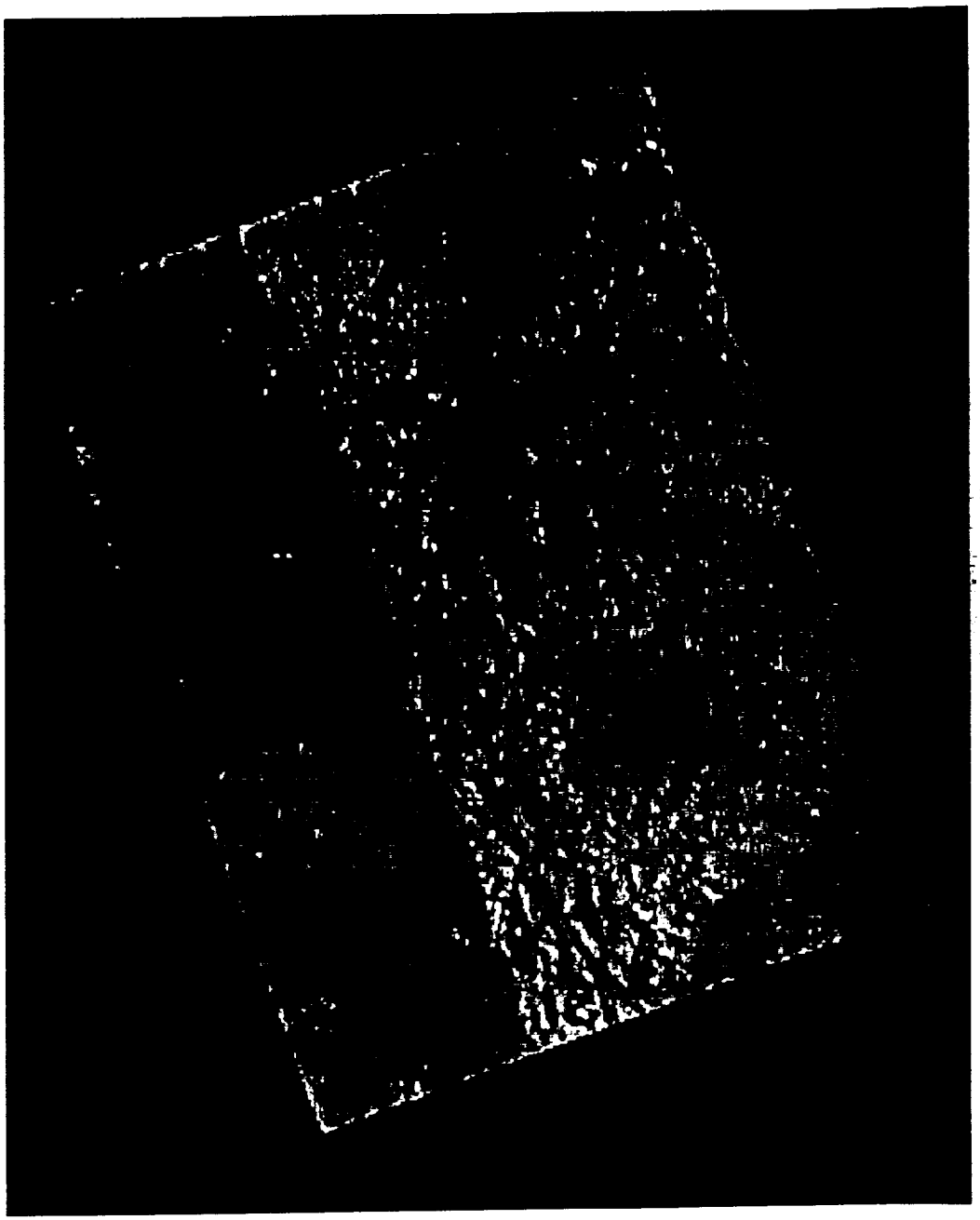

Figure 3. Terrain-effect corrected LHV image using DEM.

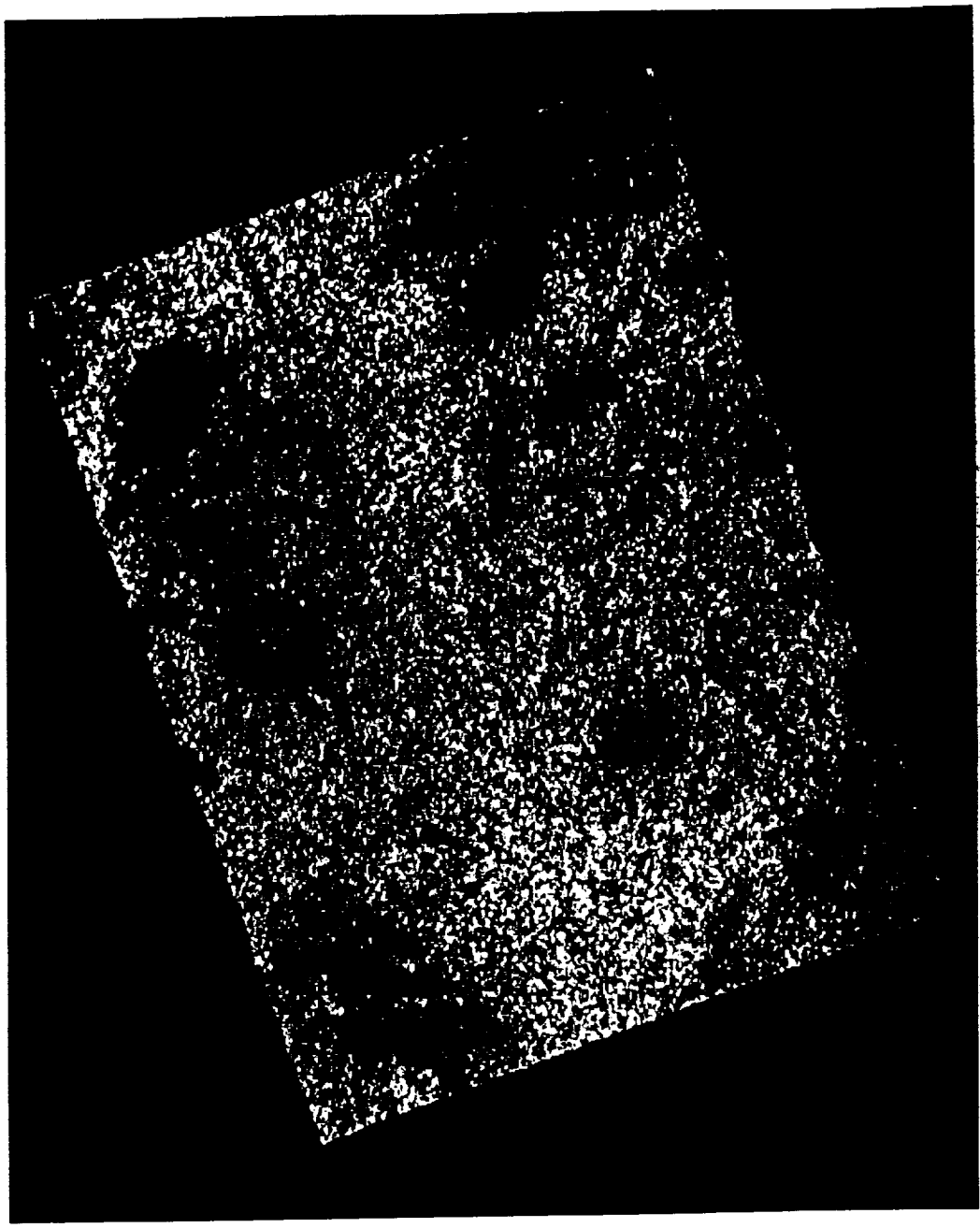

Figure 4. Composite image of Sayani test site using ratio of SIR-C Channels. LHV/LVV = red, LHV/CVV, blue = LHH/LHV.

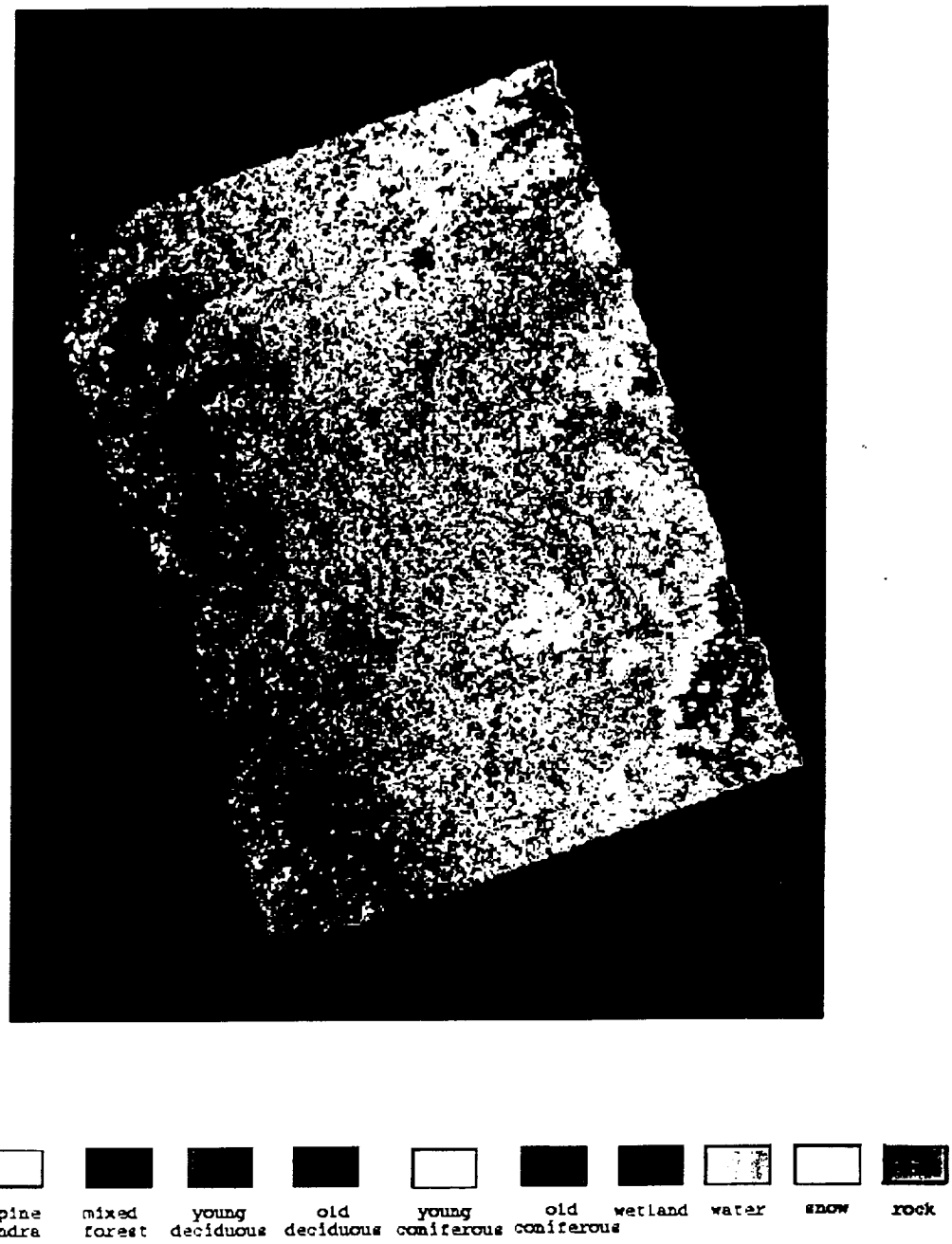

Figure 6. Classification with 6 principal components.

Figure 5. Composite image produced from first three principal components of SIR-C ratio images.